



Discovery of therapeutic agents targeting PKLR for NAFLD using drug repositioning

Downloaded from: <https://research.chalmers.se>, 2025-12-05 03:46 UTC

Citation for the original published paper (version of record):

Zhang, C., Shi, M., Kim, W. et al (2022). Discovery of therapeutic agents targeting PKLR for NAFLD using drug repositioning. *EBioMedicine*, 83. <http://dx.doi.org/10.1016/j.ebiom.2022.104214>

N.B. When citing this work, cite the original published paper.



Discovery of therapeutic agents targeting *PKLR* for NAFLD using drug repositioning

Cheng Zhang,^{a,b,1} Mengnan Shi,^{a,1} Woonghee Kim,^{a,1} Muhammad Arif,^a Martina Klevstig,^c Xiangyu Li,^a Hong Yang,^a Cemil Bayram,^d Ismail Bolat,^e Özlem Özdemir Tozlu,^f Ahmet Hacimuftuoglu,^d Serkan Yıldırım,^e Jihad Sebhaoui,^g Shazia Iqbal,^g Yongjun Wei,^b Xiaojing Shi,^b Jens Nielsen,^h Hasan Turkez,ⁱ Mathias Uhlen,^a Jan Boren,^{c,*} and Adil Mardinoglu^{a,j,*}

^aScience for Life Laboratory, KTH - Royal Institute of Technology, Stockholm, Sweden

^bSchool of Pharmaceutical Sciences & Key Laboratory of Advanced Drug Preparation Technologies, Ministry of Education, Zhengzhou University, Zhengzhou, Henan Province, 450001, PR China

^cDepartment of Molecular and Clinical Medicine, University of Gothenburg, Sahlgrenska University Hospital, Gothenburg, Sweden

^dDepartment of Medical Pharmacology, Faculty of Medicine, Atatürk University, 25240, Erzurum, Turkey

^eDepartment of Pathology, Veterinary Faculty, Atatürk University, Erzurum, 25240, Turkey

^fDepartment of Molecular Biology and Genetics, Faculty of Science, Erzurum Technical University, 25200 Erzurum, Turkey

^gTrustlife Laboratories, Drug Research & Development Center, Istanbul, Turkey

^hDepartment of Biology and Biological Engineering, Chalmers University of Technology, Gothenburg, Sweden

ⁱDepartment of Medical Biology, Faculty of Medicine, Atatürk University, Erzurum, Turkey

^jCentre for Host-Microbiome Interactions, Faculty of Dentistry, Oral & Craniofacial Sciences, King's College London, London, SE1 9RT, United Kingdom

Summary

Background Non-alcoholic fatty liver disease (NAFLD) encompasses a wide spectrum of liver pathologies. However, no medical treatment has been approved for the treatment of NAFLD. In our previous study, we found that *PKLR* could be a potential target for treatment of NAFLD. Here, we investigated the effect of *PKLR* in *in vivo* model and performed drug repositioning to identify a drug candidate for treatment of NAFLD.

Methods Tissue samples from liver, muscle, white adipose and heart were obtained from control and *PKLR* knock-out mice fed with chow and high sucrose diets. Lipidomics as well as transcriptomics analyses were conducted using these tissue samples. In addition, a computational drug repositioning analysis was performed and drug candidates were identified. The drug candidates were both tested in *in vitro* and *in vivo* models to evaluate their toxicity and efficacy.

Findings The *Pklr* KO reversed the increased hepatic triglyceride level in mice fed with high sucrose diet and partly recovered the transcriptomic changes in the liver as well as in other three tissues. Both liver and white adipose tissues exhibited dysregulated circadian transcriptomic profiles, and these dysregulations were reversed by hepatic knockout of *Pklr*. In addition, 10 small molecule drug candidates were identified as potential inhibitor of *PKLR* using our drug repositioning pipeline, and two of them significantly inhibited both the *PKLR* expression and triglyceride level in *in vitro* model. Finally, the two selected small molecule drugs were evaluated in *in vivo* rat models and we found that these drugs attenuate the hepatic steatosis without side effect on other tissues.

Interpretation In conclusion, our study provided biological insights about the critical role of *PKLR* in NAFLD progression and proposed a treatment strategy for NAFLD patients, which has been validated in preclinical studies.

Funding ScandiEdge Therapeutics and Knut and Alice Wallenberg Foundation.

Copyright © 2022 The Authors. Published by Elsevier B.V. This is an open access article under the CC BY-NC-ND license (<http://creativecommons.org/licenses/by-nc-nd/4.0/>)

Keywords: Systems biology; Drug repositioning; NAFLD; *PKLR*; Circadian rhythms

eBioMedicine 2022;83: 104214

Published online xxx
<https://doi.org/10.1016/j.ebiom.2022.104214>

*Corresponding authors at: Science for Life Laboratory, Tomtebodavägen 23A, Solna, SE-17165, Sweden.

E-mail address: adilm@scilifelab.se (A. Mardinoglu).

¹ These authors contributed equally.

Research in context

Evidence before this study

Non-alcoholic fatty liver disease (NAFLD) is a prevalent metabolic disease, and its advanced form may transform to liver cirrhosis, which has become the most common reason for liver transplantation. Regardless of its increased incidence, there is no FDA approved drug that could be used to treat NAFLD patient effectively. In our previous study, we used co-expression networks to analyse transcriptomic data of 46 of different tissues from hundreds of human subjects and identified *PKLR* as a potential liver specific target for treatment of NAFLD. *PKLR* has also been identified as a drug target for NAFLD treatment by an independent study, where co-expression networks were used to analyse the transcriptomics data of liver, muscle and adipose tissues obtained from more than one hundred different mice. We also showed that the inhibition of *PKLR* could decreased the growth of cells and steatosis level of cells by performing *in vitro* studies. Krishnan et al. recently reported that *PKLR* has a causal role in the development NAFLD based on *in vivo* studies. Therefore, there is growing evidence showing that *PKLR* is a promising target for effective treatment of NAFLD. However, at the time this study was initiated, there was very little knowledge about the response to *PKLR* suppression in the liver and other metabolic tissues, and no drug that targeting *PKLR* was developed.

Added value of this study

We for the first time investigated the *in vivo* effect of *Pklr* knockout and provided further insight about the potential of targeting *Pklr*. In addition, we reported how liver and extrahepatic tissues including white adipose, muscle and heart respond to the *Pklr* suppression in the liver in a systematic way and revealed that the *Pklr* knockout potentially regulates other tissues via circadian rhythms associated genes. Moreover, we presented a computational pipeline for drug repurposing and identified small molecule candidates that could be used to inhibit the expression of *PKLR* based on *in vitro* experiments. Finally, we show the effect of the top two selected small molecule candidates by performing *in vivo* studies and demonstrated that these candidates could be used to attenuate hepatic steatosis in rats fed with HSD without noticeable side effect on other tissues.

Implications of all the available evidence

This study showed that the knockout of *Pklr* could partly reverse the transcriptomic changes in liver, white adipose tissue, muscle and heart induced by the HSD. This study also revealed that the hepatic knockout of *Pklr* potentially affects the other tissues through circadian rhythms associated genes. The drug repositioning analysis conducted in this study proposed two promising candidates targeting *PKLR* that have been validated

extensively both in *in vitro* and *in vivo* studies. These drug candidates can be tested in future clinical studies considering the lack of drug for effective treatment of NAFLD.

Introduction

Non-alcoholic fatty liver disease (NAFLD) is defined as the accumulation of fat in the liver due to the imbalance in the uptake and secretion of fat as well as the increased *de novo* lipogenesis (DNL) or decreased oxidation of fat in the liver.¹ NAFLD can progress to non-alcoholic steatohepatitis (NASH) and it is a well-known risk factor for many metabolic diseases such as type-2 diabetes and cardiovascular disease.^{2,3} It has been reported that the prevalence of NAFLD is approximately 25% of the population, but there is no approved effective pharmacological treatment. Hence, there is an urgent need for the development of an effective treatment strategy.

Previously, we have generated gene co-expression networks (CNs) for the liver and other 45 primary human tissues, and identified the pyruvate kinase L/R (*PKLR*) as a target, whose inhibition may selectively inhibit DNL in the liver.⁴ Pyruvate kinase is a key enzyme in glycolysis and the *PKLR* gene encodes for the liver (*PKL*) and erythrocyte (*PKR*) isoforms of the enzyme and catalyses the production of pyruvate and ATP from phosphoenolpyruvate and ADP. *PKL* and *PKR* isoforms are specifically expressed in the liver and erythrocytes, respectively, and they are very lowly expressed in most of other tissues where their roles are replaced by *PKM*, which is a more commonly expressed pyruvate kinase. An independent mouse population study has also verified the driving role of *PKLR* in the development of NAFLD.⁵ Recently, we have performed *in vitro* experiments by inhibiting and overexpressing *PKLR* in HepG2 cells, and found that the expression of *PKLR* was significantly positively correlated with the expression of *FASN*, *DNL*, *TAG* levels and cell growth.⁶ In light of these findings, the integrative analysis suggested that *PKLR* could be targeted for developing a treatment strategy for NAFLD with a minimum side effect to other human tissues.

The aim of the present study is two folds: 1) investigate the driving role of *PKLR* in NAFLD progression in multi-tissue context and 2) identify potential small molecular drugs for inhibition of *PKLR*. In this study, we investigated the critical role of the *PKLR* in NAFLD in a *Pklr* knock out (KO) mouse model and revealed the underlying molecular mechanisms associated with the preventive role of *Pklr* KO in multiple tissues. In addition, we repositioned a few small molecular drugs through a computational pipeline that may modulate

expression level of *PKLR* and evaluated the top candidates in *in vitro* model. Finally, we evaluated two small molecular drugs with best performance in *in vitro* experiments in an *in vivo* rat study which follows a pre-clinical setup for promoting them into NAFLD clinical trials.

Methods

Ethics

All mice were housed at the University of Gothenburg animal facility (Lab of Exp Biomed) and supervised by university veterinarians and professional staff. The health status of our mice is constantly monitored according to the rules established by the Federation of European Laboratory Animal Science Associations. The experiments were approved by the Gothenburg Ethical Committee on Animal Experiments.

The biosafety and efficacy studies were approved by The Ethics Committee of Atatürk University, and all experiments were carried out in accordance with relevant guidelines and regulations for the care and use of laboratory animals. Animal Experiments Local Ethics Committee of Atatürk University approved the experimental procedure described in this study (Approval Date: 27.08.2020; Approval Number: 42190979- 000-E.2000208344).

Mouse animal studies

Eight male C57BL/6J mice wild-type mice and eight *Pklr*^{-/-} mutant mice were fed a standard mouse chow diet (Purina 7012, Harlan Teklad) and housed in a 12-h light–dark cycle. Only male mice were used as NAFLD is much more prevalent in male compared to female,⁷ and it has been reported that *Pklr* affects male and female mice in a gender specific way.⁸ The *Pklr* KO mice as well as the wild-type ones are purchased from Applied StemCell company. The company generated a knockout (KO) model in mouse *Pklr* gene. The model specifies a Guanine (G) deletion immediate downstream of the ATG start codon in mouse *Pklr* L-isozyme, not R-isozyme. (Supplementary report 1 & 2). From the age of 8 weeks, both the wild-type and mutant mice were then divided into two groups of 4 mice fed with chow diet, high-sucrose diet for another 8 weeks, respectively. At the age of 16 weeks, all mice are sacrificed and necropsies from liver, muscle, WAT and heart tissue were taken for RNA sequencing and lipid quantification.

All mice were housed at the University of Gothenburg animal facility (Lab of Exp Biomed) and supervised by university veterinarians and professional staff. The health status of our mice is constantly monitored according to the rules established by the Federation of European Laboratory Animal Science Associations. The experiments were approved by the Gothenburg Ethical Committee on Animal Experiments.

Rat animal studies

In vivo biosafety studies. Healthy Sprague Dawley male rats (12 weeks old, 260–300 g) were obtained from Atatürk University Experimental Research Center (ATADEM, Erzurum Turkey) and housed under standard environmental conditions (temperature 20 °C–25 °C, humidity 50 ± 20% and 12-hour light/dark diurnal cycle). Food and water were available *ad libitum*. Rats were randomly separated into one control group and two experimental groups (30 mg/kg/day BX-912 or JNK-IN-5A, n=5). BX-912 and JNK-IN-5A were dissolved in DMSO and were orally administrated using oral gavage for 7 days. The control group were received the same amount of vehicle solution only. The weights of the rats are provided in Table S1.

After 7 days, rats were anaesthetized and blood samples were collected from the abdominal aorta for biochemical and hematological analysis. The plasma was separated and stored at –80 °C for further analysis. Major organs such as: heart, kidney, liver, muscle, adipose, intestine (duodenum, ileum, jejunum), pancreas, colon, and stomach were collected from all the animals for further analysis. Selected organs were fixed in 10% neutral buffered formalin for histopathological examination.

In addition to sampling for biochemical and hematological analysis, one drop of blood samples was obtained from the animals for evaluating micronucleus frequencies as genotoxicity endpoint at the end of the experiments. Three different smears of each rat were prepared using pre-coded and cold slides, then the slides air-dried at room temperature, and fixed in ethanol for 10 min, and stained with Giemsa. The frequencies of micro nucleated polychromatic erythrocytes (MNPCEs) were analyzed according to previously suggested approach using a light microscope. The incidence of MN-PCEs was determined by scoring a total of 3000 PCE per animal and results were expressed as % MN.⁹

In vivo efficacy studies. After 1-week acclimation period, rats were randomly separated into two groups: control group (n=5) and high sucrose group (n=20). The control group was fed with a standard diet while the others consumed high sucrose diet (HSD). Sucrose was purchased from Sigma Chemical Co. (St Louis, MO, USA) and supplied at the dose of 10% in the drink water for two weeks. The consumption of sucrose water and weights of the rats are provided in Table S1.

After 2 weeks, five rats in the HSD group were randomly sacrificed for conformation of NAFLD model. Then, the remaining rats in the HSD group were separated into 3 sub-groups (n=5): HSD group, HSD plus BX-912 group and HSD plus JNK-IN-5A group. BX-912 and JNK-IN-5A were dissolved in DMSO and were orally administrated using oral gavage for one week (30 mg/kg/day). HSD group was treated with vehicle solution only.

At the end of the experiment, rats were sacrificed after being anesthetized. Blood samples were collected from the abdominal aorta and centrifuged at 8000 rpm for 15 min at 4 °C. The plasma was separated and stored at -80 °C until further analysis. Other internal organs, including the heart, adipose tissues, liver, kidney, muscle, intestine (duodenum, ileum, jejunum), pancreas, colon and stomach were immediately removed and then snap frozen in liquid nitrogen and stored at -80 °C; the liver was also fixed in 10% formaldehyde for histopathological examination.

The biosafety and efficacy studies were approved by The Ethics Committee of Atatürk University, and all experiments were carried out in accordance with relevant guidelines and regulations for the care and use of laboratory animals. Animal Experiments Local Ethics Committee of Atatürk University approved the experimental procedure described in this study (Approval Date: 27.08.2020; Approval Number: 42190979- 000-E.2000208344).

Histopathological examination. The liver tissues were fixed in 10% buffered formaldehyde solution. After fixation, the tissues were passed through graded alcohol and xylene series and embedded in paraffin blocks. 5 micrometer thick sections were taken serially from the paraffin blocks. Histopathological changes were evaluated by performing hematoxylin eosin staining on the sections taken. Sections were evaluated according to histopathological findings as none (-), mild (+), moderate (++) and severe (+++).

Immunohistochemical examination. After deparaffinization, the slides were immersed in antigen retrieval solution (pH6.0) and heated in microwave for 15 min to unmask the antigens. The sections were then dipped in 3% H₂O₂ for 10 min to block endogenous peroxidase activity. Protein block was dropped onto the sections, washed with PBS for 10 min. Primary antibodies (8-OH-dG, Cat No: sc-66036, Diluent Ratio: 1/100, Santa Cruz) were prepared and applied according to the usage conditions. Expose mouse and rabbit specific HRP/DAB detection IHC kit were used as follows: sections were incubated with goat anti-mouse antibody, then with streptavidin peroxidase, and finally with 3,3' di-amino benzidine + chromogen. Slides were counter stained with hematoxylin. Immunoreactivity in the sections were graded as none (-), mild (+), moderate (++) and severe (+++).

Cell experiments

WT HepG2 was included in this study and cultured by Roswell Park Memorial Institute (RPMI, R2405, Sigma Aldrich) 1640 Medium with 10% fetal bovine serum (FBS) and 1% penicillin – streptomycin (PS). To induce a steatosis model into WT HepG2 cells, high glucose Dulbecco's Modified Eagle Media (DMEM, D0822/ D5671, Sigma-Aldrich) containing 10% FBS and 1% PS was used as medium for one week, together with 10 µg/

mL insulin and 10 µM T0901317. All of cells were incubated in the incubator with 5% CO₂ and 37 °C (Thermo SCIENTIFIC). Fresh medium was provided every two days.

Nine drugs were tested in this study and all of them were bought from commercial companies as shown in Table S2. All the drugs were diluted in Dimethyl sulfoxide (DMSO, 41639, Sigma-Aldrich) and stored in -20 °C.

As for drug-screening, different numbers of HepG2 cells were seeded for distinct experiments. More in details, 40,000 cells and 500,000 cells were used for 2-day-drug treatment in 96-well-plate and 6-well plate, respectively, while 80,000 cells and 300,000 cells were used for one-week drug treatment in 96-well plate and 6-well plate, respectively. Detailed drug dosages could be found in Table S3. Fresh medium was provided every two days.

Transcriptomic data from human patients

We validated the key genes we identified in mouse fed with HSD by performing differential expression analysis for the publicly available human patient datasets where the study details and its characteristics are also reported.¹⁰

RNA extraction and sequencing

Total RNA was isolated from homogenized heart tissue using RNeasy Fibrous Tissue Mini Kit (Qiagen). cDNA was synthesized with the high-capacity cDNA Reverse Transcription Kit (Applied Biosystems) and random primers. mRNA expression of genes of interest was analyzed with TaqMan real-time PCR in a ViiATM 7 system (Applied Biosystems). RNA sequencing library were prepared with Illumina RNA-Seq with Poly-A selections. Subsequently, the libraries were sequenced on NovaSeq6000 (NovaSeq Control Software 1.6.0/RNA v3.4.4) with a 2 × 51 setup using 'NovaSeqXp' workflow in 'S1' mode flow cell. The Bcl was converted to FastQ by bcl2fastq_v2.19.1.403 from CASAVA software suite (Sanger/phred33/Illumina 1.8+ quality scale).

Lipid quantification

Lipids were extracted as described previously (Lofgren et al, 2012). Internal standards were added during the extraction. Lipids were analysed using a combination of HPLC and mass spectrometry as described (Stahlman et al, 2013). Briefly, straight-phase HPLC was used to purify ceramides (CER). Cholesteryl ester (CE), triacylglycerol (TAG), phosphatidylethanolamine (PE), phosphatidylcholine (PC), and sphingomyelin (SM) were quantified using a QTRAP 5500 mass spectrometer (Sciex, Concord, Canada) equipped with a robotic nanoflow ion source, TriVersa NanoMate (Advion Bio-Sciences, Ithaca, NJ). CER were analysed using reversed-phase HPLC coupled to a triple-quadrupole

Quattro Premier mass spectrometer (Waters, Milford, MA, USA).

Western blot

Protein content levels were detected by western blot. After the respective treatment of drugs, the cells pellet was lysed in cell lysis M, followed by protein extraction from supernatant (10 min, 13,000 r/min centrifuge). Extracted cell lysate was stored in -20°C. Proteins were quantified through Bovine albumin serum (BAS) standard curve with protein assay dye reagent (BIO-RAD). The proteins were separated by SDS-PAGE with 100V in 90 min by mini-protein TGX precast gels (4-15%, 15 wells, 15 µl/well, BIO-RAD), and then transfer to Mini PVDF transfer package through transfer system (Transfer-Turbo, BIO-RAD). After 30 min blocking with 5% skim milk in cold room (4°C) and washing with TBST, membrane was cut by the size of interested proteins. Primary antibodies were added into the corresponding membrane sections for overnight binding. Then the membranes were washed with TBST, and the secondary antibodies were incubated for 1 h in cold room. The following antibody were used: (Goat pAb to Rb Ig, ab205718, abcam; Rb pAb to beta-actin, ab8227, abcam; anti-pklr, HPA006653, SIGMA; Rb pAb to fatty acid synthase, ab9539, abcam). The binds were imaged by immunostaining and machine (ImageQuant LAS 500). All of the antibodies were purchased from Abcam online, and β -actin was used as global normalized protein. After measurement, the strength of signal for each protein was quantified by ImageJ. The background noise was removed, and all of the results were normalized by the levels of β -actin.

Cell viability assay & Triglyceride assay for in vitro experiment

Cell viability and lipids content were detected on the same batch of cells. After one-week treatment of drugs in steatosis model, drug cytotoxicity was determined by Cell Counting Kit 8 (CCK-8, Sigma-Aldrich), and triglyceride levels were detected by Triglyceride Quantification Assay (TAG) kit (Abcam, ab65336). Then the absorbance was measured at 450 nm and 570 nm, respectively. To normalize triglyceride content level, average values of cell viability were applied.

Transcriptomics data

The raw RNA-sequencing results were processed using Kallisto¹¹ with index file generated from the Ensembl mouse reference genome (Release-92).¹² The output from Kallisto, both estimated count and TPM (Transcript per kilobase million), were subsequently mapped to gene using the mapping file retrieved from Ensembl BioMart website, by filtering only protein coding genes and transcripts. Genes with mean expression less than 1

TPM in each condition were filtered. For data exploration, we used PCA from sklearn package (<https://dl.acm.org/doi/10.5555/1953048.2078195pi>) in Python 3.7 and used TPM values as the input.

Subsequently, we performed differential gene expression analysis using DESeq2 package in R.¹³ To define a gene as differentially expressed (DEGs), a gene has to fulfil a criterion of FDR < 5%. The results of differential expression analysis were then used for functional analysis.

We performed functional analysis using the R package PIANO.¹⁴ As the input, we used the fold changes and p-values from the DESeq2, and also KEGG pathways gene-set collections from Enrichr. To define a process or pathway as significant, we used a cut off of FDR < 10% for the distinct direction of PIANO (both up and down).

Identification of *Pklr* gene signature

The *Pklr* signature was determined by meta-analysis of three individual RNA-seq datasets. The first two datasets were obtained from our previous study⁶ where we used siRNA/plasmid to inhibit/over-express *Pklr* in HepG2 cell line, respectively. Raw sequencing data was mapped by Kallisto based on GRCh38 (genome v23). We performed differential expression analysis with R package DESeq2 for the two datasets. The results of DEGs were recognized as gene signature, which respectively referred to *Pklr* inhibition signature and *Pklr* over-expression signature hereafter. Next, we collected RNA-seq data of liver biopsies from 110 healthy donors generated by the Genotype-Tissue Expression (GTEx) project. After removing low expressed genes (TPM < 1), we calculated the spearman correlation coefficient between *Pklr* and other genes, referred to *Pklr* co-expression signature. In summary, we detected three *Pklr*-related gene signature, namely *Pklr* co-expression signature (N = 11733), *Pklr* inhibition signature (N = 16399) and *Pklr* over-expression signature (N = 14903).

The next step was to generate a *Pklr* consensus signature by aggregating the three-candidate gene lists. First of all, genes were defined as *Pklr* positively related genes if they met three conditions at the same time: positive log₂ fold change values in *Pklr* over-expression signature group; negative log₂ fold change values in *Pklr* inhibition signature group; positive correlation coefficient in *Pklr* co-expression signature. The definition of *Pklr* negatively correlated genes was the opposite. These *Pklr* positively/negatively correlated genes generated a list of *Pklr* consensus correlated genes (N=4994).

To rank these consensus genes by the level of relationship with *Pklr* in a uniform standard, we calculated a combined z-score for them by aggregating the P-values from the three lists of *Pklr* signature. Specifically,

for each list of P-values, we transformed the P-Values (two-tailed significance test) to z-score as follow:

$$p = 2\Phi\left(-|Z|\right)$$

where Φ is the standard normal cumulative distribution function.¹⁵

Then we calculated a combined z-score for 4998 combined *PKL* correlated genes. The equation is as follow:

$$Z_{IVW} = \frac{\bar{X}}{SE(\bar{X})} = \frac{\sum_i^W X_i}{\sqrt{\sum_i^W}}$$

where X is the z score from three independent results and W is the weight (set as 1 for all of three results) and IVW is the Inverse variance-weighted (IVW) average method.¹⁵

Consequently, we were able to order the 4998 *Pklr* consensus correlated genes by the aggregated z-scores, and these z-scores were defined as our final *Pklr* consensus signature (Table S4). Notably, z-scores of negatively correlated genes were labelled as negative values and vice versa, in order to reflect the direction of genes.

Drug repositioning

The fifth level of LINCS L1000 phase 2 data were downloaded (GEO: GSE70138) and used for detecting the connectivity of small molecules and gene signatures.¹⁶ HepG2 cell line data was specifically parsed from the whole file, containing differential expressed gene signatures after small molecules' treatment. Then the Spearman correlation coefficient was calculated between our *Pklr* consensus signatures and these drug-perturbed gene signatures, focusing on the 3698 pair-wised genes (Table S4). P-Values were adjusted based on the Benjamini-Hochberg method. Drugs were ranked by r value, and we considered top 10 drugs as potential *Pklr* inhibitors ($r < -0.4$, FDR < 1E-95). In total, there were 10 drugs extracted, and nine of them that we could purchase were selected for wet lab validation afterward.

RRIDs

RRID tags for all cell lines, model organisms and antibodies are provided in Table S5.

Data and code availability

All raw RNA-sequencing data generated from this study can be accessed through accession number GSE. Codes used during the analysis are available on <https://github.com/sysmedicine/pklr>.

Statistics

All experiments' results were shown by mean \pm SD and calculated by T-test, and $p < 0.05$ was considered as significance on comparison across different groups. In

mice and rat experiment, four mice and five rats were applied for each group as biological replicates, respectively. In HepG2 experiments, all measurements were performed three times independently. Adjusted p-values were applied for transcriptomic data analysis, which was calculated through the False Discovery Rate (FDR).

Role of funding source

The funders of the study had no role in study design, data collection, data analysis, data interpretation, or writing of the report.

Results

The effect of PKLR KO on liver

To systematically investigate the effect of pyruvate kinase liver isoform in multi tissue context, we fed four groups of 8-week-old *Pklr* KO and control C57Bl/6J mice (Ctrl) either with HSD or CHOW for eight weeks (Figure 1A).

We carefully examined the liver and plasma lipid levels as well as the fatty acids composition in all four groups of mice (Figure 1B-I). We found that HSD-fed mice developed significant liver fat compared to CHOW-fed mice (Figure 1B). The *Pklr* KO mice were well tolerant of the HSD and *Pklr* KO HSD-fed mice had significantly lower liver TG levels than the Ctrl HSD-fed mice (Figure 1B). In addition, we found that the hepatic level of ceramide, lactosylceramide and sphingomyelin levels were significantly decreased in *Pklr* KO mice compared to the Ctrl Chow-fed mice (Figure 1C-E). We also found lysophosphatidylcholine, sphingomyelin, phosphatidylcholines and phosphatidylethanolamine are significantly increased in *Pklr* KO HSD-fed mice compared to the Ctrl HSD-fed mice (Figure 1E&F). No significant changes in plasma cholesterol or triglycerides we observed between *Pklr* KO and Ctrl mice (Figure 1G&H), and notably, a significant decrease of saturated fatty acids percentage in *Pklr* KO HSD-fed mice compared to the Ctrl HSD-fed mice (Figure 1I).

To systematically study how the *Pklr* KO prevent the development of liver fat in mice fed with HSD, we collected liver tissue samples from these four groups of mice and generated RNA-seq data. We firstly examined the hepatic *Fasn* expression and found that it is significantly elevated in Ctrl HSD-fed mice but not in the *Pklr* KO HSD-fed mice (Figure 2A). Our analysis indicated that *Pklr* KO inhibits the hepatic DNL in HSD-fed mice. We found that there is no significant difference in the *Fasn* expression between the *Pklr* KO CHOW-fed mice and Ctrl CHOW-fed mice, and this is also supported by the measurement of comparable liver TG levels between these two groups of mice (Figure 1B).

Next, we focused on two comparisons, Ctrl HSD-fed vs Ctrl CHOW-fed and *Pklr* KO HSD-fed vs Ctrl HSD-

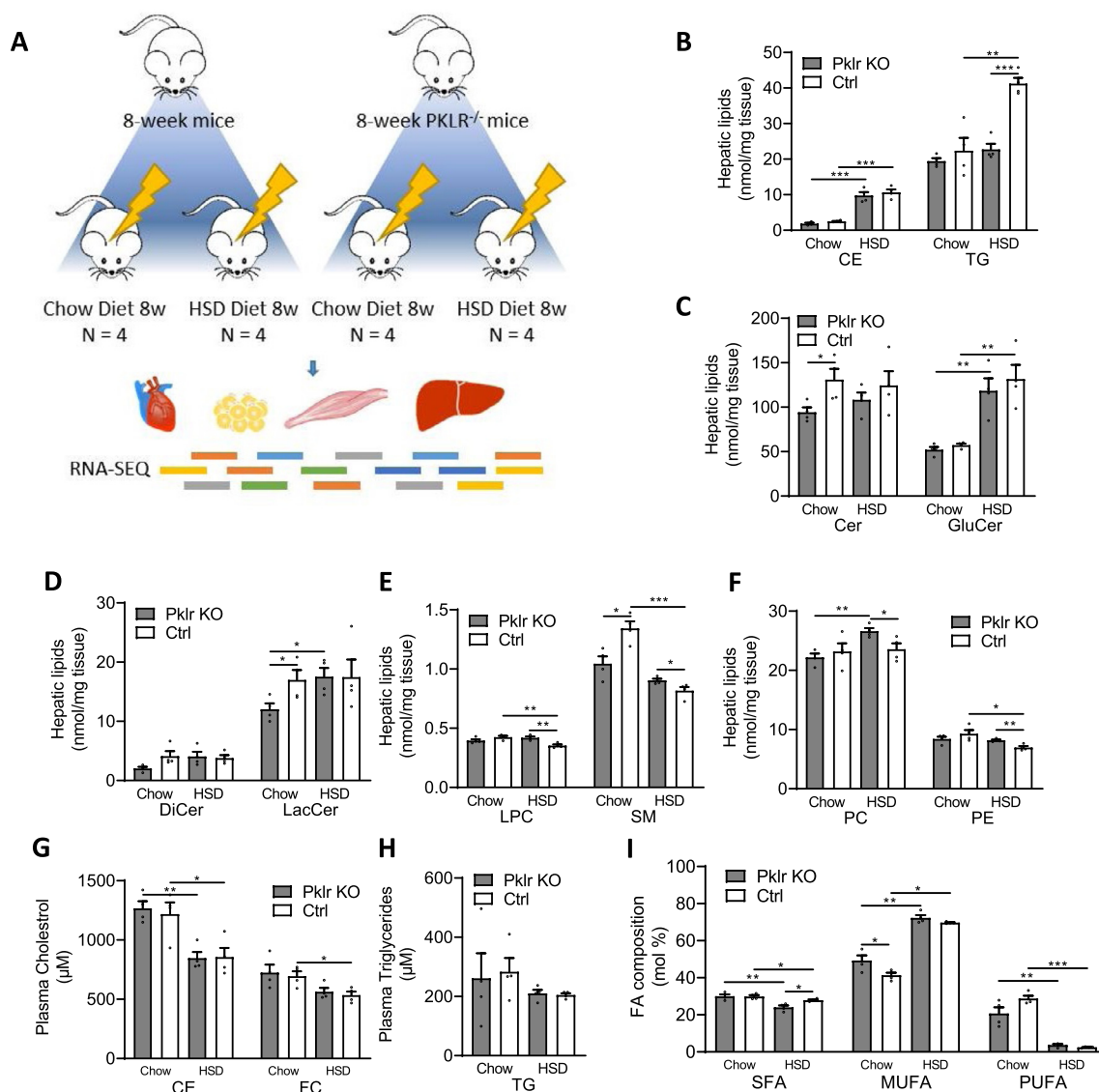


Figure 1. Analysis for liver lipidomics profile of 8-week wild-type and *Pklr* KO mice fed with CHOW and HSD. (A) Flow chart showing the experimental design. (B-F) Bar graphs showing the hepatic cholesterol ester (CE), triacylglyceride (TG), ceramide (Cer), glucosylceramide (GluCer), dihydroceramides (DiCer), lactosylceramide (LacCer), lysophosphatidylcholines (LPC), sphingomyelin (SM), phosphatidylcholines (PC) and phosphatidylethanolamine (PE) levels of mice in different conditions. (G-H) Bar graphs showing the plasma cholesterol ester (CE), free cholesterol (FC) and triacylglyceride (TG) levels of mice in different conditions. (I) Bar graph showing the composition of saturated fatty acids (SFA), mono unsaturated fatty acids (MUFA) and poly unsaturated fatty acids (PUFA) levels of mice in different conditions. * $P < 0.05$, ** $P < 0.01$, *** $P < 0.001$.

fed mice and analyzed the transcriptomic changes between high liver fat vs normal as well as *Pklr* KO treatment vs high liver fat, respectively. We performed differential expression analysis and pathway enrichment analysis using KEGG pathways. We identified 957 DEGs between Ctrl HSD-fed vs Ctrl CHOW-fed mice and 90 DEGs between *Pklr* KO HSD-fed vs Ctrl HSD-fed mice (Figure S1; Table S6). Interestingly, we found that 58 DEGs are shared between these two groups and

showed a significant transcriptomic change in the opposite direction (hypergeometric $P = 0$; Figure 2B). We performed functional enrichment analysis using these 58 overlapped DEGs and found that these genes are significantly enriched in circadian rhythms ($P_{adj.} < 0.05$; Figure 2C; Table S7), which suggests the *Pklr* KO reversed the dysregulation of circadian rhythms induced by HSD. Notably, the expression level of these DEGs in the circadian rhythms pathway is not significantly

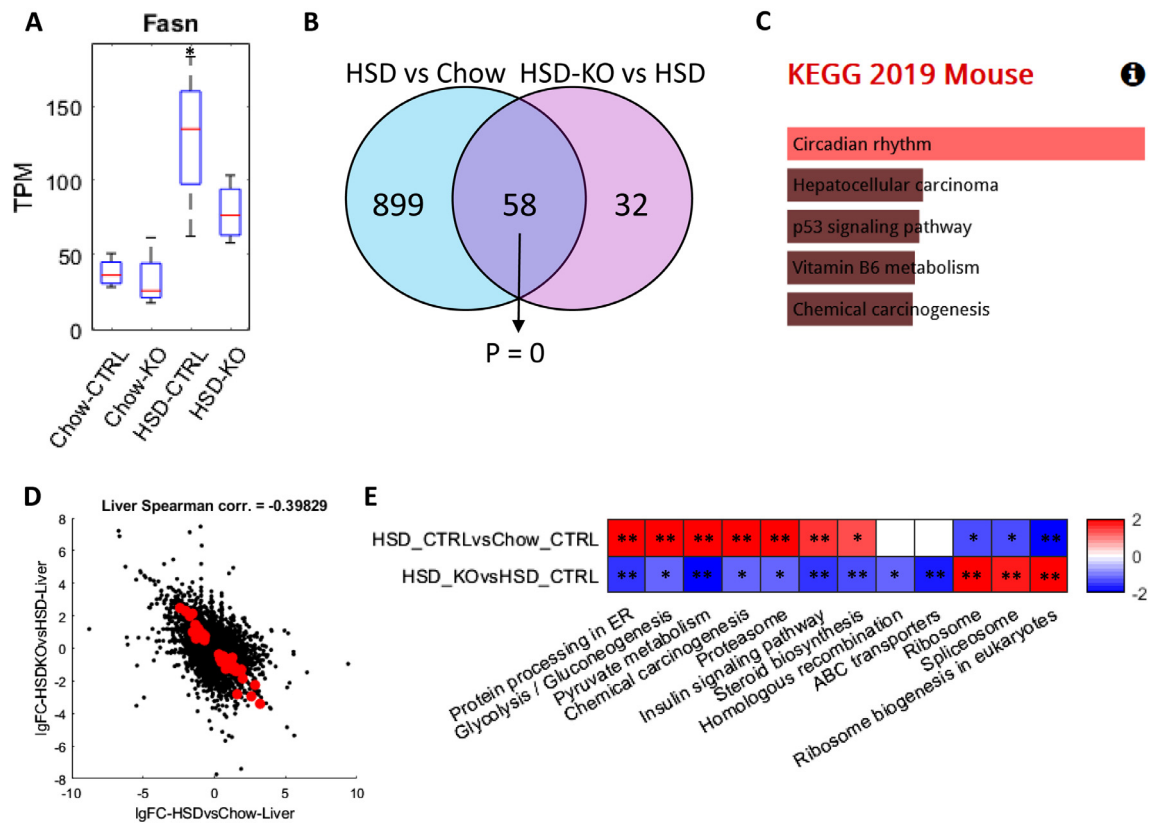


Figure 2. Analysis for liver transcriptomics profile of 8-week wild-type and *Pklr* KO mice fed with CHOW and HSD. (A) Box plot showing the expression of *Fasn* in different conditions, and the asterisks indicated the significant increase of *Fasn* expression compared to wild-type mice fed with CHOW ($P < 0.05$). (B) Venn-diagram showing the number and hypergeometric P value of overlapped DEGs between HSD Ctrl vs CHOW Ctrl and HSD Ctrl vs HSD KO in liver. (C) Barplot showing the significantly enriched KEGG pathways of the overlapped DEGs in Figure 2B. (D) Scatter plot showing the correlation between the log 2 fold changes of gene expression of all genes in HSD Ctrl vs CHOW Ctrl (x-axis) and HSD KO vs HSD Ctrl (y-axis), where the dots highlighted in red are the overlapped DEGs highlighted in Figure 2B. (E) Heatmap showing the differentially expressed pathways in the two comparisons, respectively, where each cell in the plot shows the minus log 10 P value if they are up-regulated, and positive log 10 P value if they are down-regulated (* P adj. < 0.1 ; ** P adj. < 0.05). Only pathways that are significantly differentially expressed in HSD KO vs HSD Ctrl (P adj. < 0.1) are displayed and pathways without significant expression alterations (P adj. > 0.1) are marked white.

altered in the *Pklr* KO mice compared with the wild-type mice fed with CHOW (P adj. > 0.05 ; Table S5).

We analyzed the transcriptomic changes' landscape and found an apparent negative correlation between the fold changes of the transcriptomic expression between these two comparisons (Spearman corr. = -0.398; Figure 2D). We also employed the PIANO toolbox¹⁴ to investigate the pathway level transcriptomic changes based on the KEGG pathways.¹⁷ The pathway-level changes we identified in HSD vs CHOW included up-regulation of glycolysis, insulin signaling pathway, protein processing in ER, fatty acid metabolism, steroid and terpenoid metabolism and down-regulation of amino acid metabolism and transcription (Figure S2). Although less number of pathways showed significant alteration in the *Pklr* KO HSD-fed compared to Ctrl HSD-fed mice, the transcriptomic expression of several

these pathways, such as protein processing in ER, glycolysis, insulin signaling pathway, steroid biosynthesis, ribosome and spliceosome pathways, are significantly reversed after *Pklr* KO (Figure 2E).

Investigating NAFLD progression and *Pklr* KO effect in other metabolic tissues

It has been reported that the progression of NAFLD is associated with extrahepatic tissues, such as WAT, muscle and heart tissues.¹⁸ Hence, it is vital to analyse the global transcriptomics changes in multi-tissue context to study the molecular differences during NAFLD progression and *Pklr* KO. We obtained WAT, muscle and heart tissue samples from the 8-week Ctrl and *Pklr* KO mice fed with both CHOW and HSD and generated RNA-Seq data. First, we performed differential expression analysis between Ctrl HSD-fed vs Ctrl CHOW-fed

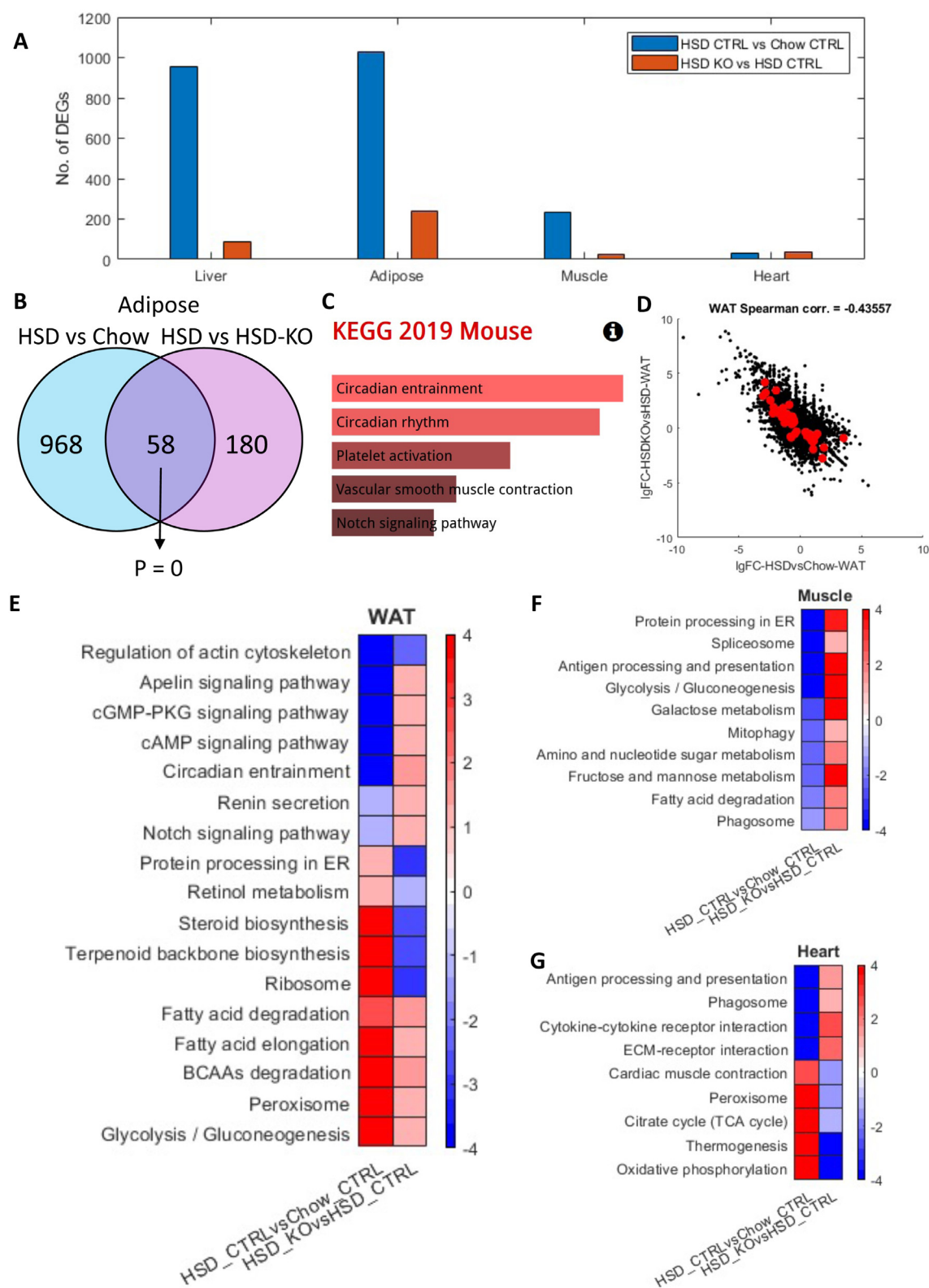


Figure 3. Analysis for transcriptomics profile of muscle, WAT and heart obtained from 8-week wild-type and PKI KO mice fed with different CHOW and HSD. (A) Bar graph showing the number of DEGs in indicated comparisons liver, WAT, muscle and heart.

and *Pklr* KO HSD-fed vs Ctrl HSD-fed mice in these three tissues and compared them with the DEGs in the liver (Figure 3A and Figure S1 & S3; Table S5).

Interestingly, we observed the largest number of DEGs in WAT among all comparisons (1026 and 238, respectively), followed by the muscle (236 and 5, respectively) and heart (32 and 2, respectively). We checked the overlapped DEGs between the two comparisons (Ctrl HSD-fed vs Ctrl CHOW-fed and *Pklr* KO HSD-fed vs Ctrl HSD-fed) in WAT and found that 58 genes are significantly reversely altered (hypergeometric $P = 0$; Figure 3B), which is very similar to what we observed in the liver. Interestingly, we found the master circadian regulators, *Clock* and *Arntl* (*Bmal1*), are second and third most down-regulated genes and *Per3*, which is also a key player in circadian rhythms, is among the top 10 up-regulated genes in *Pklr* KO HSD-fed vs Ctrl HSD-fed within the 58 overlapped genes. In addition, although not statistically significant, the top two enriched KEGG pathways of these 58 genes are circadian entrainment and circadian rhythm (FDR = 0.17; Table S8). This is in excellent agreement with the 58 altered DEGs in the liver (Figure S4). Hence, our analysis indicated that circadian regulation play an important role in the whole-body response to *Pklr* KO. It should be noted that 3 genes, namely *Per3*, *Npas2* and *Cldn1*, are shared between the two 58 overlapped DEGs both in the liver and adipose tissues. Both *Per3* and *Npas2* are key players in circadian rhythms, and this further signifies the role of *Pklr* KO in circadian regulation. Moreover, we observed a negative correlation between the fold changes of the gene expressions between these two comparisons (Spearman corr. = -0.436; Figure 3D). We also investigated the changes in muscle and heart tissues. Notably, the DEGs are also significantly reversely overlapped in the muscle and heart tissues (hypergeometric $P < 0.05$) and their gene expression changes also showed negative correlations as well (Figure S5). Taken together, we observed that the hepatic *Pklr* KO partly reversed the transcriptomic changes in extrahepatic tissues induced by HSD.

Next, we investigated the pathway level changes using the DEGs in all three tissues using PIANO and KEGG pathways in the same way as in the liver tissue. In WAT, we observed significant up-regulation of protein processing in ER, ribosome, retinol metabolism and steroid and terpenoid backbone biosynthesis pathways and significant down-regulation of several

signaling pathways, such as cAMP signaling, notch signaling, cGMP-PKG signaling, apelin signaling pathways between Ctrl HSD-fed vs Ctrl CHOW-fed mice. These pathways are significantly changed in the opposite direction between *Pklr* KO HSD-fed vs Ctrl HSD-fed mice (Figure 3E). These pathways with the reversed gene expression changes indicated the changes in WAT in response to *Pklr* KO. For instance, the reverse of steroid and terpenoid backbone biosynthesis pathways implicated the potential link between *Pklr* and whole-body steroid hemostasis. Notably, in both Ctrl HSD-fed vs Ctrl CHOW-fed and *Pklr* KO HSD-fed vs Ctrl HSD-fed mice, glycolysis, peroxisome, BCAAs degradation, fatty acid degradation and elongation pathways are significantly up-regulated in WAT, while regulation of actin cytoskeleton pathway is significantly down-regulated. The gene expression changes in these pathways are enhanced rather than reversed with *Pklr* KO, suggesting the complementary response of these pathways to the hepatic gene expression changes. This is exemplified by the enhanced up-regulated glycolysis pathway, as its up-regulation in Ctrl HSD-fed vs Ctrl CHOW-fed mice is probably caused by the excessive amount of glucose intake in the diet. The up-regulation in *Pklr* KO HSD-fed vs Ctrl HSD-fed mice implicated that the decreased glucose intake in the liver in response to *Pklr* KO is complemented by the further enhanced glycolysis in WAT.

In the muscle tissue, we observed that the *Pklr* KO reversed the down-regulation of metabolic pathways, including glycolysis, galactose metabolism, fructose and mannose metabolism, amino and nucleotide sugar metabolism and fatty acid degradation, and other pathways such as protein processing in ER, antigen processing and presentation, mitophagy, phagosome and spliceosome pathways. In the heart tissue, the *Pklr* KO reversed the down-regulation of antigen processing and presentation, phagosome, cytokine-cytokine receptor and ECM-receptor interaction pathways and attenuated the expression of the up-regulated pathways, including cardiac muscle contraction, peroxisome, TCA cycle, thermogenesis, oxidative phosphorylation. Notably, no pathway in muscle or heart showed enhanced transcriptomic changes after *Pklr* KO in response to HSD. In summary, we concluded that the *Pklr* KO reversed the transcriptomic changes induced by HSD in extrahepatic tissues, and the affected pathways are mostly related to protein processing, carbohydrate metabolism, fatty

(B) Venn-diagram showing the number and hypergeometric P value of overlapped DEGs between HSD Ctrl vs CHOW Ctrl and HSD Ctrl vs HSD KO in WAT. (C) Barplot showing the significantly enriched KEGG pathways of the overlapped DEGs in Figure 4B. (D) Scatter plot showing the correlation between the log 2 fold changes of gene expression of all genes in HSD Ctrl vs CHOW Ctrl (x-axis) and HSD KO vs HSD Ctrl (y-axis), where the dots highlighted in red are the overlapped DEGs highlighted in Figure 4B. (E-G) Heat-maps showing the differentially expressed pathways in the two comparisons in WAT, muscle and heart, respectively, where each cell in the plot shows the minus log 10 P value if they are up-regulated, and positive log 10 P value if they are down-regulated (* P adj. <0.1; ** P adj. <0.05). Only pathways that are significantly differentially expressed in both HSD KO vs HSD Ctrl and HSD Ctrl vs CHOW Ctrl (P adj. <0.1) are displayed.

acids metabolism, and oxidative phosphorylation as well as some immune and cell recognition associated pathways.

Drug repositioning for inhibition of *Pklr* in vitro

Based on the *in vivo* experiments, we concluded that *PKLR* is a promising drug target to treat NAFLD. Therefore, we performed drug repositioning and identified therapeutic agents that can modulate *PKLR*. In this context, we developed a computational pipeline for repositioning of small molecule drugs that can effectively inhibit *PKLR* expression using the data in the Connectivity Map.¹⁶ (Figure 4A). In brief, we analysed human liver tissue RNA-Seq data obtained from 110 subjects in the GTEx database and HepG2 cell line RNA-Seq data where we inhibited/over-expressed *PKLR*, and identified a *PKLR*-related consensus gene signature (Table S4). We compared this consensus gene signature with the gene expression profiles of more than 1800 compound-perturbed-HepG2 from the LINCS L1000 database and identified the potential inhibitors that show similar gene expression profile (see method). As a result, we selected the 10 drugs with the most negative expression correlation with the *PKLR*-related consensus gene signature and identified these drugs as potential *PKLR* inhibitors (Table S9).

We evaluated all 10 drugs by performing a literature review (Table S2) and found some of these drugs have been associated with fatty acid metabolism. For instance, Azacitidine, which was reported as a DNA methyltransferase inhibitor, has been approved by the US FDA for the treatment of all subtypes of myelodysplastic syndromes (MDS)¹⁹ It has also been found that the drug reduces the expression level of a list of genes controlling fatty acid biosynthesis and *Pcsk9* expression based on *in vitro* experiments.²⁰ In the high-glucose-cultured HepG2 cell model, the agent decreases the expression level of another key DNL gene, *Fasn*.²¹ Among the other 9 compounds, six of them turned out to be kinase inhibitors, indicating their potential effect on *PKLR*. Additionally, AS-601245 and JNK-IN-5A were reported as the kinase inhibitor of c-Jun N-terminal kinases (JNK).²²

To determine the inhibitory effects of drugs on the expression level of *PKLR*, HepG2 was selected as the *in vitro* model for coherence. We purchased nine drugs (BX-912, PLX-4720, QL-XII-47, Azacitidine, CGK-733, AS-601245, PF-477736, JNK-IN-5A, Dabrafenib) from the list that are commercially available and treated HepG2 cells with these drugs for two days with different dosages due to their potential cellular toxicities (Table S3), and then measured the *PKLR* protein level by western blotting. The protein expression levels of *PKLR* were compared between the drug-treated and Ctrl group after normalizing with β -actin. As shown in Figure 4B, six of the nine tested drugs significantly down-regulated the protein expression of *PKLR* ($P < 0.05$).

To further analyse the effect of these drugs on lipid accumulation via the DNL pathway, we induced steatosis to HepG2 by treating the cells with high glucose medium (DMEM), insulin and To901317 (see Method).²³ After 7 days of drug treatment, eight of the nine tested drugs significantly decreased the protein expression level of *PKLR* ($P < 0.05$; Figure 4C). Six of the nine tested drugs also significantly reduced the protein expression level of *FASN* ($P < 0.05$; Figure 4D). Specifically, BX-912 and JNK-IN-5A treated groups showed a dramatic reduction in the protein expression level of both *PKLR* and *FASN* in the steatosis model. Therefore, we investigated the effects of these two drugs on the *de novo* synthesis of lipids based on the steatosis-induced HepG2 model. After 7 days of drug treatment, both drugs significantly decreased the content of TGs in the HepG2 cells (Figure 4E). Taken together, we showed that BX-912 and JNK-IN-5A effectively alleviate the protein expression of *PKLR* and *FASN* as well as TG levels in HepG2 cell lines, and thus, we decided to perform *in vivo* evaluations to test the effect of these two drugs.

The treatment of rats with the therapeutic agents

To evaluate the potential toxicity of BX-912 and JNK-IN-5A in animals, we raised three groups of 12-week-old rats ($n = 5$), fed the first group with CHOW (Ctrl), the second group with CHOW plus BX-912 (30 mg/kg) and the third group with CHOW plus JNK-IN-5A (30 mg/kg) for seven days (Figure 5A). After 7 days, all rats were sacrificed, and tissue samples from major organs and blood samples were collected for biosafety evaluation. We analysed the frequencies of micro nucleated polychromatic erythrocytes (MNPCEs) in the blood samples, and found that the frequencies of MNPCEs in drug-treated groups were not statistically different ($p > 0.05$) when compared to Ctrl animals. Our analysis indicated that both tested agents exhibited non-genotoxic potential (Figure 5B; Table S10). In addition, we performed histopathological examinations using the tissue samples obtained from the rats and found that kidney, small intestine, large intestine, stomach, heart, pancreas, muscle tissues and liver from all three rat groups exhibited normal histological structures (Figure 5C and D). Moreover, we performed immunohistochemical (IHC) examination on the liver tissues from the rats and observed negative 8-OH-dG expression in all three groups. Therefore, we concluded that both BX-912 and JNK-IN-5A have no side effects on tissues obtained from the rats.

Next, we investigated the efficacy of these two drugs in a steatosis rat study by feeding the animals with HSD. We raised five groups of 12-week-old rats ($n = 5$) and fed the first group with CHOW diet and the remaining four groups with HSD for two weeks (Figure 6A). At the end of week 2, we sacrificed the CHOW-fed rats

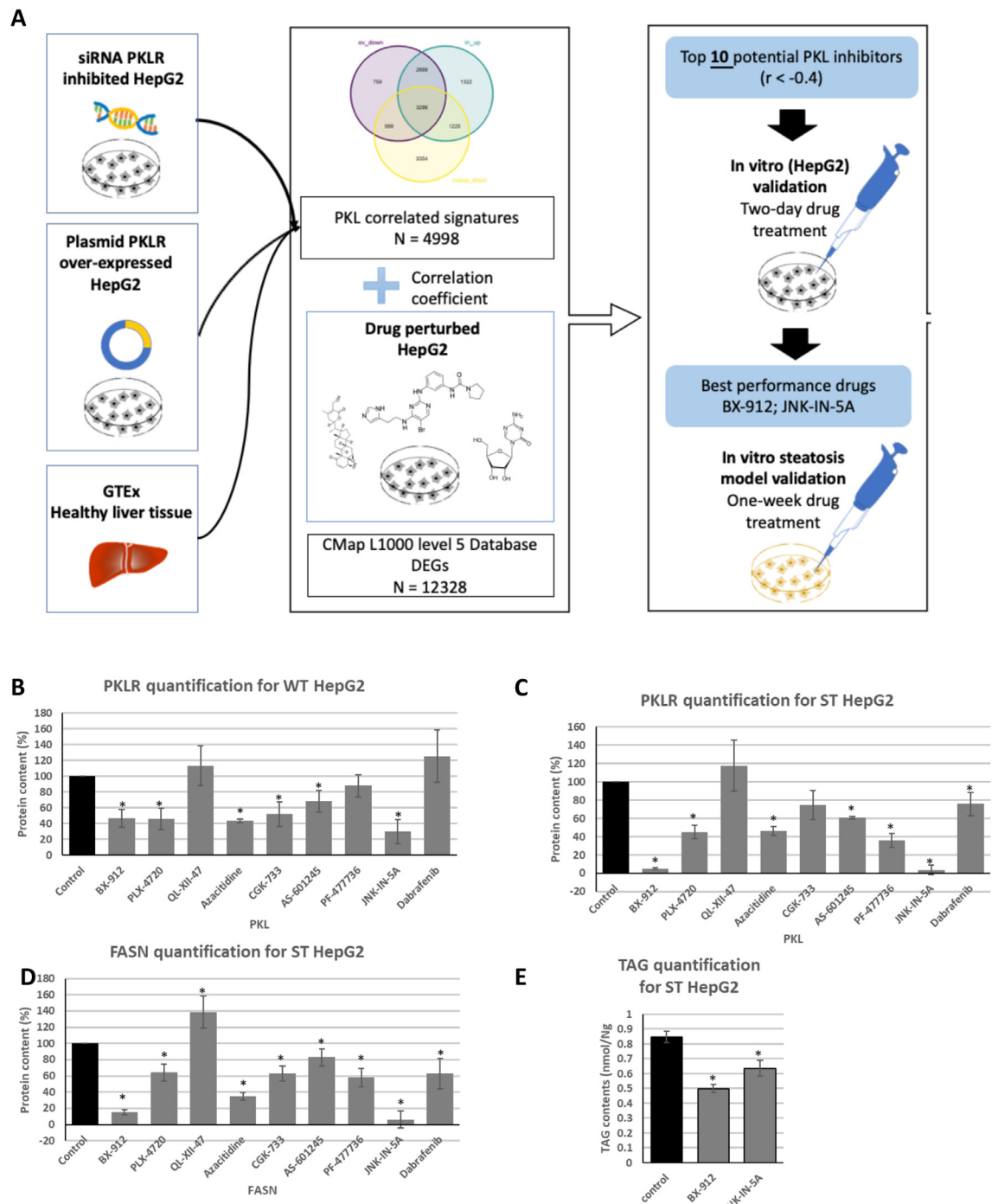


Figure 4. Drug repositioning application and in vitro validation of potential PKLR inhibitors. (A) Workflow. (B-D) Bar plot showing the drug effects on protein expression of HepG2 and steatosis-induced HepG2, normalized by β -actin. (E) Bar plot showing the drug effects on triglyceride contents of steatosis-induced HepG2. The results were normalized by cell viability. Results were normalized by protein content. (G) Bar plot showing the results of western blot of liver biopsy, normalized by β -actin. (*: p-value < 0.05; t-test)

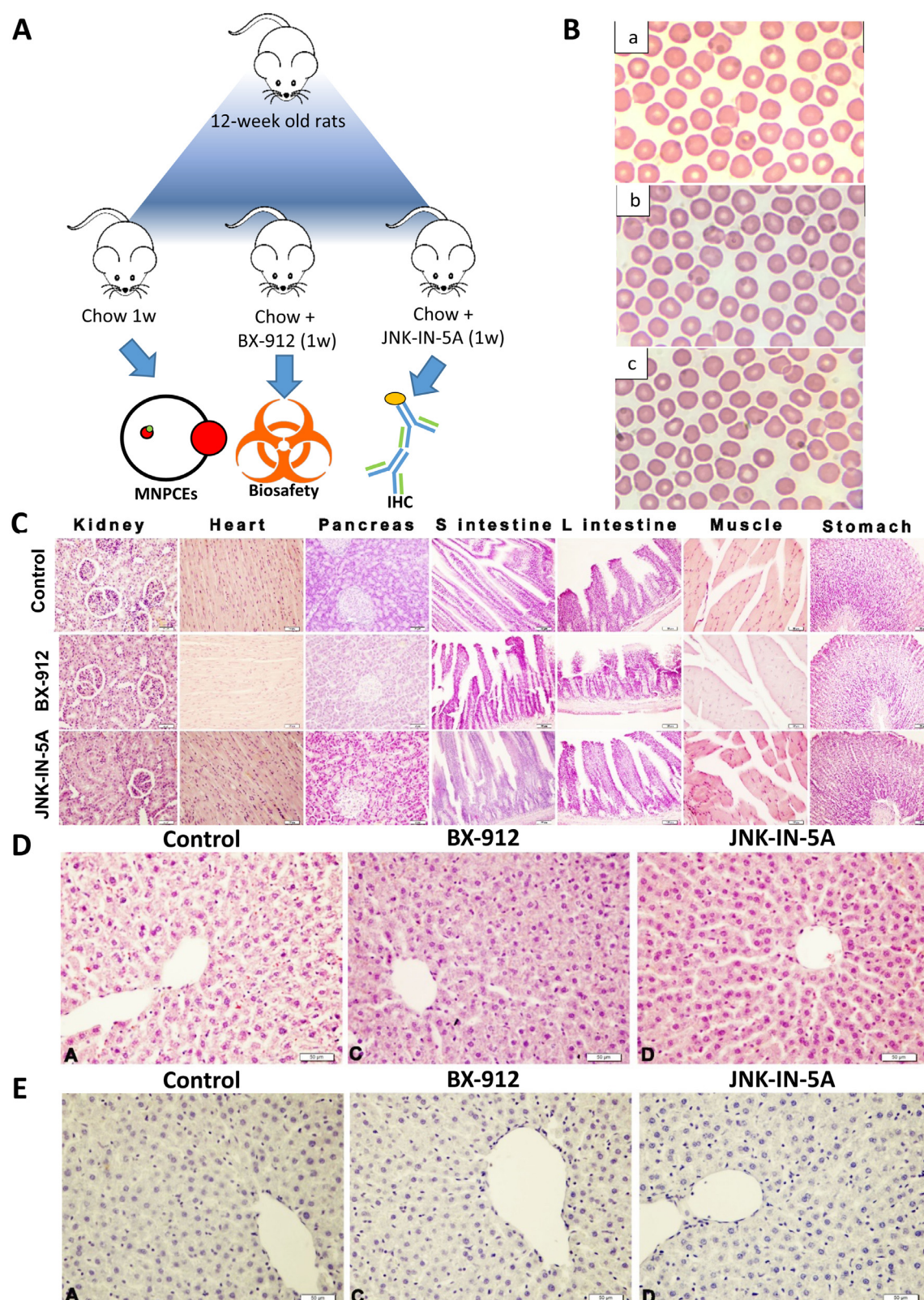


Figure 5. In vivo biosafety examination of the potential PkIr inhibitors. (A) Workflow. (B) Light micrograph of rat blood smear obtained from (a) control group (b) treated with 30 mg/kg BX-912 (c) treated with 30 mg/kg JNK-512 for 7 days (Giemsa stain,

(n = 5) and HSD-fed rats (n = 5) for histopathological examination and confirmed the HSD fed rats already developed hepatic steatosis.

After securing the development of the liver steatosis model, we fed the third group with HSD (HSD 3w), the fourth group with HSD plus BX-912 (30 mg/kg) and the fifth group with HSD plus JNK-IN-5A (30 mg/kg) for 7 days. After 7 days, all three groups of rats were sacrificed, and tissue samples from the liver and other major organs and blood samples were collected for efficacy examination. We performed a histopathological and IHC analysis on the liver samples and other major organs obtained from the three rat groups. We observed a standard histological structure on the small intestine, large intestine, stomach, heart and muscle tissues in the examination for drug-treated groups and found no toxic effect of the small molecule drugs on these tissues (Figure 6B). In the rats from HSD 3w group, severe degeneration was detected in the renal tubule epithelium and severe fattening was detected in the parenchyma cells in the pancreatic tissues. Interestingly, we detected only mild degeneration in renal tubule epithelium and mild fattening in the parenchyma cells of pancreas tissues in drug-treated groups. In addition, we observed severe degeneration and severe steatosis in hepatocytes in liver tissues of rats from the HSD 3w group, mild degeneration and moderate steatosis in hepatocytes in liver tissues of the HSD-fed rats treated with BX-912, while observed only mild degeneration and mild steatosis in the liver tissues of the HSD-fed rats treated with JNK-IN-5A (Figure 6C; Table S11). Moreover, we observed strong 8-OH-dG expression in hepatocytes in liver tissues of the rats from HSD 3w group and found the 8-OH-dG expression is significantly decreased in drug-treated groups compared to the HSD 3w rats (Figure 6D; Table S11).

Discussions

Based on our mice experiment, we observed that *Pklr* KO in liver could prevent the HSD-induced hepatic steatosis and functional alterations at transcriptomic level. Based on the lipidomics data, we found that the *Pklr* KO group could help in reversing the hepatic TG level elevated by HSD to a level that is similar in the liver of mice fed with Chow diet. We also observed that the mRNA expression level of glycolysis, steroid biosynthesis and insulin signaling pathways are enhanced in the livers of HSD-fed mice and these effects have been attenuated in the livers of *Pklr* KO HSD-fed mice.

Enhancement of glycolysis and insulin resistance is a hallmark of NAFLD,²⁴ and the inhibition of these two pathways in *Pklr* KO mice highlighted the potential role of *Pklr* as a therapeutic target for NAFLD treatment. In fact, a recent study transfected shRNA and plasmid to respectively inhibit and over-express *Pklr* in the liver of mice, and demonstrated that *Pklr* has a causal role in developing insulin resistance.⁸ In addition, the reverse effect of the steroid biosynthesis suggested a potential link between hepatic *Pklr* and steroid hormone homeostasis, known to be involved in the development of NAFLD.²⁵

Apart from the decreased hepatic TG level, we also found the hepatic level of several lipid species are elevated in the liver of *Pklr* KO in HSD fed mice, namely lysophosphatidylcholine (LPC), sphingomyelin (SM), phosphatidylcholines (PC) and phosphatidylethanolamine (PE). Previous studies reported that LPC could induce hepatocyte lipoapoptosis,^{26,27} and the elevated LPC may be a potential side effect of *Pklr* KO. However, considering that the LPC level of the HSD-fed *Pklr* KO mice is marginal and has no significant differences compared to the ctrl mice fed with Chow diet, no severe toxic effect is expected. SM can be converted to ceramide through the sphingomyelinase pathway, and the decrease of ceramide level could probably explain the increased SM in the HSD fed *Pklr* KO mice compared to the ctrl mice. PC is widely used in the regression of liver steatosis,²⁸ and thus, its elevation is potentially a positive indication. Lower hepatic PC to PE ratio has been reported as a risk factor for NAFLD,²⁹ but since both PC and PE are increased, the increased PE did not change the PC to PE ratio significantly.

Our study also for the first time reported the *Pklr* KO effect in liver and other extrahepatic tissues. Our results provided valuable insights about the biological function of *Pklr* in the whole-body context. We found that the most responsive extrahepatic tissue is WAT. Many pathways showed significant transcriptomic alteration including glycolysis, steroid biosynthesis, protein processing in ER and ribosome pathways which is very similar to those observed in liver and implicated a synergistic regulation between liver and WAT. Interestingly, central circadian regulators also showed similar alterations based on transcriptomics data, which may implicate that *Pklr* induces the transcriptomic changes in WAT via synchronization of circadian rhythms. It is known that circadian clock includes glucose sensor and participates in the orchestration of glucose homeostasis.³⁰ and it has been reported that interruption of circadian

1,000x magnification). (C) Histological images from major organs of the indicate rat groups where Control, BX and JNK represents rats fed with chow diet, chow diet plus BX-912 and chow diet plus JNK-IN-5A, respectively. (D) Histological images from liver tissue samples from respective rat groups where arrows and arrowheads respectively indicate degeneration and steatosis. Bar: 50µm. (E) IHC images with staining showing 8-OH-dG expression indicated by arrowheads in liver tissues from corresponding rat groups.

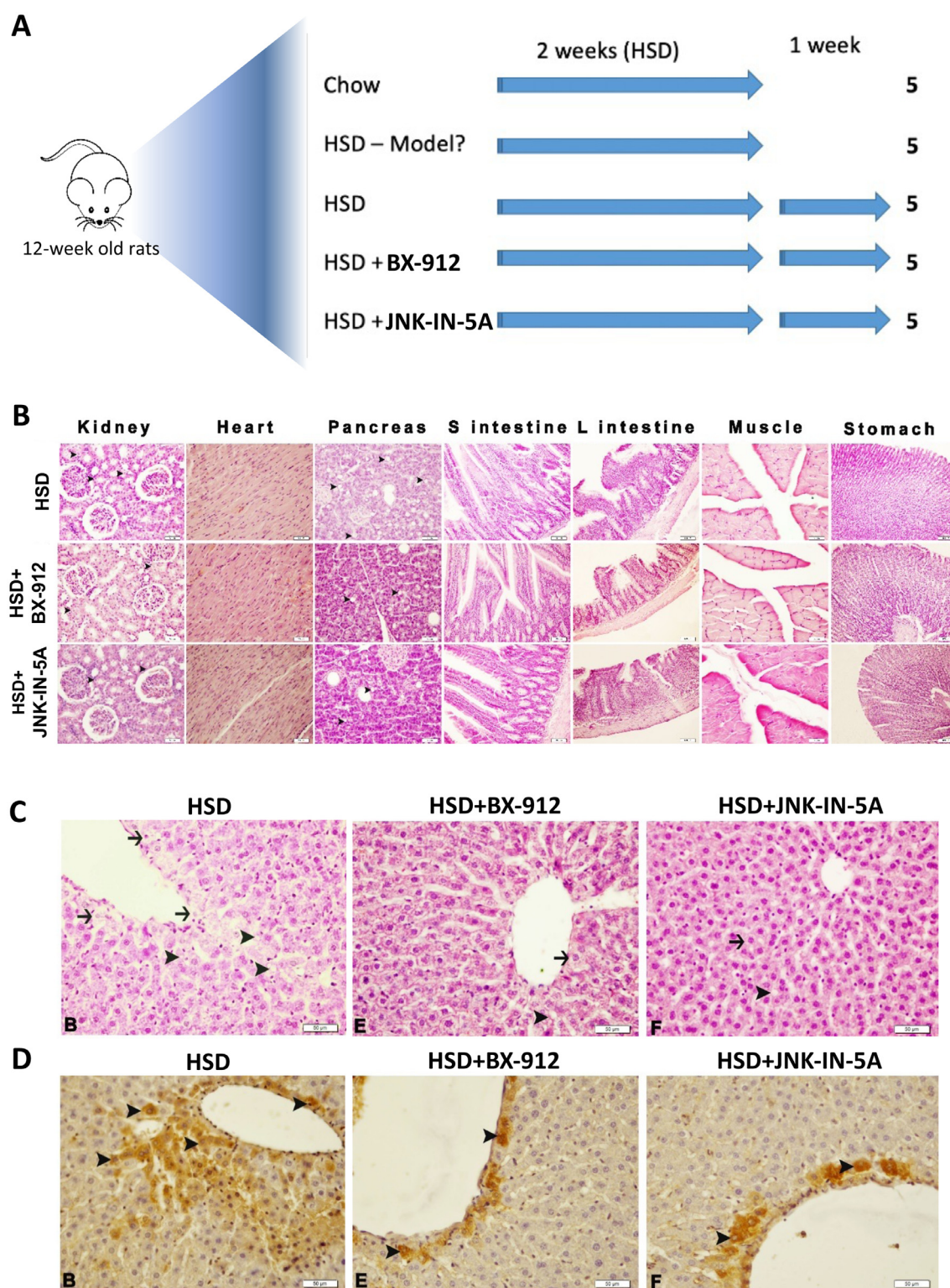


Figure 6. In vivo efficacy experiment for the potential Pklr inhibitors. (A) Study design of the experiment. (B) Histological images from liver tissue samples from respective rat groups where arrows and arrowheads respectively indicated degeneration and steatosis. Bar: 50µm. (C) IHC images with staining showing 8-OH-dG expression indicated by arrowheads in liver tissues from corresponding rat groups. (D) Bar plot illustrating the triglyceride contents of liver biopsy of drug-treated mice. (E) Bar plot showing the hepatic protein expression of indicated proteins quantified by western blot, normalized by β -actin. (*: p-value < 0.05; t-test)

rhythms might be an important contributor to the development of insulin resistance.³¹ In addition, a previous study reported the liver specific knockout of *Bmal1*, which is the key circadian regulator, disrupted the diurnal rhythms of hepatic *Pklr* expression.³² Previous studies and our analysis may indicate the regulatory effect between the key circadian regulator and *Pklr* in the liver. In this context, it is possible that the *Pklr* KO could directly affect the circadian rhythm in the liver. Moreover, both liver and WAT have autonomous circadian clocks which are regulated partly by glucose intake, and it is very likely for liver to synchronize its circadian clock with the WAT one via controlling glucose and lipid metabolism.³¹ Taken together, we speculated that the excessive intake of glucose in HSD-fed mice disrupts the circadian regulation and induces insulin resistance in liver and WAT. The knockout of *Pklr* inhibits the glycolysis in liver and restores the circadian rhythms in the liver and WAT. Our previous study already showed that inhibiting *PKLR* in human liver cells could decrease their glucose intake⁶ and could partly support the role of *PKLR* in glycolysis, but future study that investigate its mechanistic role in circadian rhythms in whole-body context is needed.

To identify a small molecule drug that could potentially be used to treat NAFLD via inhibition of *Pklr*, we established a computational drug repositioning pipeline and found 10 candidate drugs that could modulate *Pklr*. Unlike traditional method, the identified drugs were meant to decrease the expression of the target gene rather than its activity. We validated the inhibitory effect on *Pklr* expression as well as lipid accumulation of the six predicted drugs in an *in vitro* steatosis model. In addition, the two most effective small molecules drugs, namely BX-912 and JNK-IN-5A, were tested in rat animal study. Both drugs passed biosafety experiment in rat without causing noticeable side effect in the animals. In addition, we observed that both drugs significantly decreased liver fat and attenuated oxidative stress, degeneration of renal tubule epithelium and fattening in the parenchyma cells of pancreatic tissues in the rats, implicating a whole-body improvement of the rats which agrees well with what we observed in the multi-tissue transcriptomic analysis. These results highlighted the efficiency and power of computational drug repositioning pipeline.

In summary, our study demonstrated that knockout of *Pklr* prevent HSD-fed mice from developing liver fat by effecting liver, WAT, muscle, and heart tissues. We showed that the *Pklr* KO could reverse the HSD induced pathway transcriptomic changes and observed that these changes could be regulated via metabolically synchronized circadian rhythms. We also identified two small molecule drugs, which inhibit the *Pklr* expression and attenuate the liver fat *in vivo*. Therefore, our study provided biological insights about the effect of *Pklr* KO *in vivo*, and presented the development of a promising

therapeutic solution for treatment of NAFLD patients, which should be evaluated in additional animal biosafety evaluations and future clinical trials.

Limitations

A potential limitation in this study is that we used rat as *in vivo* model for validation of the drug repositioning instead of mouse which was used earlier in this study. Ideally, the same animal model could be used throughout the study, but we selected rat model for evaluation of the drug effect as it is a more commonly used preclinical model for biosafety and drug efficacy tests. Considering that the increased hepatic steatosis and inflammation (oxidative stress) were observed also in the HSD-fed rats, we concluded that the HSD fed rats could serve as a proper model for studying NAFLD as well as evaluating the drug effects.

Contributors

C.Z., M.S., W.K., M.A., X.L., Y.W., X.S. J.N., H.T., M.U., J.B. and A.M. conducted the data analyses and interpretation. H.Y. M. S. performed the drug repositioning analyses. W.K. and M.K. measured the expression of genes in the mouse tissue samples. M.S. and W.K. performed the experiment to evaluate screened drugs. M.K. performed the mouse experiment. C.B., I.B., Ö.Ö.T., A. H., S.Y., J. S., S. I. and H.T. performed the biosafety and efficacy experiment on rats. M.U., J.B. and A.M. supervised the study. C.Z. and A.M. wrote the manuscript, and all co-authors edited the manuscript. All authors approved the final version of the manuscript, and C.Z., M.S. and W.K. have verified the underlying data.

Data sharing statement

All raw RNA-sequencing data generated from this study can be accessed through accession number GSE193627 used during the analysis are available on <https://github.com/sysmedicine/pklr>. Additional results or methods generated by this study is potentially available upon request to the corresponding author.

Declaration of interests

AM, JB and MU are the founder and shareholders of ScandiEdge Therapeutics and they filed a patent application on the use of small molecules to treat NAFLD patients. The other authors declare no competing interests.

Acknowledgement

This work was financially supported by ScandiEdge Therapeutics and Knut and Alice Wallenberg Foundation.

The computations and data handling were enabled by resources provided by the Swedish National

Infrastructure for Computing (SNIC) at UPPMAX, partially funded by the Swedish Research Council through grant agreement no. 2018-05973.

Supplementary materials

Supplementary material associated with this article can be found in the online version at doi:10.1016/j.ebiom.2022.104214.

References

- Gluchowski NL, Becuwe M, Walther TC, Farese Jr. RV. Lipid droplets and liver disease: from basic biology to clinical implications. *Nat Rev Gastroenterol Hepatol*. 2017;14(6):343–355.
- Mardinoglu A, Uhlen M, Boren J. Broad views of non-alcoholic fatty liver disease. *Cell Syst*. 2018;6(1):7–9.
- Tana C, Ballestri S, Ricci F, et al. Cardiovascular risk in non-alcoholic fatty liver disease: mechanisms and therapeutic implications. *Int J Environ Res Public Health*. 2019;16(17):3104.
- Lee S, Zhang C, Liu Z, et al. Network analyses identify liver-specific targets for treating liver diseases. *Mol Syst Biol*. 2017;13(8):938.
- Chella Krishnan K, Kurt Z, Barrere-Cain R, et al. Integration of multi-omics data from mouse diversity panel highlights mitochondrial dysfunction in non-alcoholic fatty liver disease. *Cell Syst*. 2018;6(1):103–115.e7.
- Liu Z, Zhang C, Lee S, et al. Pyruvate kinase L/R is a regulator of lipid metabolism and mitochondrial function. *Metab Eng*. 2019;52:263–272.
- Pan JJ, Fallon MB. Gender and racial differences in nonalcoholic fatty liver disease. *World J Hepatol*. 2014;6(5):274–283.
- Chella Krishnan K, Floyd RR, Sabir S, et al. Liver pyruvate kinase promotes NAFLD/NASH in both mice and humans in a sex-specific manner. *Cell Mol Gastroenterol Hepatol*. 2021;11(2):389–406.
- Solorzano-Melendez A, Rodrigo-Alarcon R, Gomez-Meda BC, et al. Micronucleated erythrocytes in peripheral blood from neonate rats fed by nursing mothers exposed to X-rays. *Environ Mol Mutagen*. 2021;62(3):177–184.
- Govaere O, Cockell S, Tiniakos D, et al. Transcriptomic profiling across the nonalcoholic fatty liver disease spectrum reveals gene signatures for steatohepatitis and fibrosis. *Sci Transl Med*. 2020;12(572):eaba4448.
- Bray NL, Pimentel H, Melsted P, Pachter L. Near-optimal probabilistic RNA-seq quantification. *Nat Biotechnol*. 2016;34(5):525–527.
- Zerbino DR, Achuthan P, Akanni W, et al. Ensembl 2018. *Nucleic Acids Res*. 2018;46(D1):D754–D761.
- Love MI, Huber W, Anders S. Moderated estimation of fold change and dispersion for RNA-seq data with DESeq2. *Genome Biol*. 2014;15(12):550.
- Varemo L, Nielsen J, Nookaew I. Enriching the gene set analysis of genome-wide data by incorporating directionality of gene expression and combining statistical hypotheses and methods. *Nucleic Acids Res*. 2013;41(8):4378–4391.
- Lee CH, Cook S, Lee JS, Han B. Comparison of two meta-analysis methods: inverse-variance-weighted average and weighted sum of Z-scores. *Genomics Inform*. 2016;14(4):173–180.
- Subramanian A, Narayan R, Corsello SM, et al. A next generation connectivity map: L1000 platform and the first 1,000,000 profiles. *Cell*. 2017;171(6):1437–1452.
- Kanehisa M, Furumichi M, Sato Y, Ishiguro-Watanabe M, Tanabe M. KEGG: integrating viruses and cellular organisms. *Nucleic Acids Res*. 2021;49(D1):D545–D551.
- Haas JT, Francque S, Staels B. Pathophysiology and mechanisms of nonalcoholic fatty liver disease. *Annu Rev Physiol*. 2016;78:181–205.
- Muller A, Florek M. 5-Azacytidine/azacitidine. *Recent Results Cancer Res*. 2010;184:159–170.
- Poirier S, Samami S, Mamarbachi M, et al. The epigenetic drug 5-azacytidine interferes with cholesterol and lipid metabolism. *J Biol Chem*. 2014;289(27):18736–18751.
- Hosseini H, Teimouri M, Shabani M, et al. Resveratrol alleviates non-alcoholic fatty liver disease through epigenetic modification of the Nrf2 signaling pathway. *Int J Biochem Cell Biol*. 2020;119:105667.
- Cerbone A, Toaldo C, Pizzimenti S, et al. AS601245, an anti-inflammatory JNK inhibitor, and clofibrate have a synergistic effect in inducing cell responses and in affecting the gene expression profile in CaCo-2 colon cancer cells. *PPAR Res*. 2012;2012:269751.
- Hansmann F, Mordier S, Iynedjian PB. Insulin induction of glucokinase and fatty acid synthase in hepatocytes: analysis of the roles of sterol-regulatory-element-binding protein-1c and liver X receptor. *Biochem J*. 2006;399(2):275–283.
- Fabbri E, Sullivan S, Klein S. Obesity and nonalcoholic fatty liver disease: biochemical, metabolic, and clinical implications. *Hepatol*. 2010;51(2):679–689.
- Charni-Natan M, Aloni-Grinstein R, Osher E, Rotter V. Liver and steroid hormones-can a touch of p53 make a difference? *Front Endocrinol*. 2019;10:374.
- Han MS, Park SY, Shinzawa K, et al. Lysophosphatidylcholine as a death effector in the lipopoptosis of hepatocytes. *J Lipid Res*. 2008;49(1):84–97.
- Kakisaka K, Cazanave SC, Fingas CD, et al. Mechanisms of lysophosphatidylcholine-induced hepatocyte lipopoptosis. *Am J Physiol Gastrointest Liver Physiol*. 2012;302(1):G77–G84.
- Osipova D, Kokoreva K, Lazebnik L, et al. Regression of liver steatosis following phosphatidylcholine administration: a review of molecular and metabolic pathways involved. *Front Pharmacol*. 2022;13:797923.
- Arendt BM, Ma DW, Simons B, et al. Nonalcoholic fatty liver disease is associated with lower hepatic and erythrocyte ratios of phosphatidylcholine to phosphatidylethanolamine. *Appl Physiol Nutr Metab*. 2013;38(3):334–340.
- Asher G, Schibler U. Crosstalk between components of circadian and metabolic cycles in mammals. *Cell Metab*. 2011;13(2):125–137.
- Stenvers DJ, Scheer F, Schrauwen P, la Fleur SE, Kalsbeek A. Circadian clocks and insulin resistance. *Nat Rev Endocrinol*. 2019;15(2):75–89.
- Udoh US, Valcin JA, Swain TM, et al. Genetic deletion of the circadian clock transcription factor BMAL1 and chronic alcohol consumption differentially alter hepatic glycogen in mice. *Am J Physiol Gastrointest Liver Physiol*. 2018;314(3):G431–G447.